Contents

1. Introduction

Surgical resection is the first and most effective therapeutic choice for pancreatic cancer that is localized without distant metastases. Although extended surgery with portal vein resection has been attempted, the survival rate for patients who have undergone resection for pancreatic cancer is still very low (8–25%) [1–4]. One reason is that pancreatic cancer cells, which easily invade and develop into the extrapancreatic nerve plexus and lymph vessels, remain in the pancreatic bed (the retroperitoneal space) even after curative resection, and subsequently induce local recurrence at a high incidence [5–8]. Intraoperative radiotherapy as an adjuvant treatment has been used to try to reduce local recurrence, but its effectiveness is still under debate [9–11]. When detected clinically, local recurrence is mostly difficult to treat, because it occurs at a deep area in the body and has already established a tumor mass, which has physiological and environmental resistance to chemotherapy and radiotherapy [12,13]. The most critical timing of treatment for the prevention of local recurrence must be immediately after resection during surgery, prior to tumor mass formation derived from remnant cancer cells.

Regarding the environment of remnant cancer cells after surgery, surgical wounds induce inflammation and regeneration of tissues with an increased level of cytokines that provides favorable conditions for tumor recurrence [14–17]. That is, cytokines, which are produced and exist in a tumor-resected tissue and in the intraperitoneal space due to surgical trauma, such as hepatocyte growth factor (HGF), epidermal growth factor (EGF), basic fibroblast growth factor (bFGF), transforming growth factor-β (TGF-β) and vascular endothelial growth factor (VEGF), accelerate cancer cell proliferation, migration, invasion and tumor angiogenesis, resulting in recurrence and metastasis of cancer (Fig. 1). This is a well-accepted scenario of recurrence of pancreatic cancer.

To suppress the progress of cancer cells, there must be two main strategies; one is cytostatic therapy using a cytokine antagonist or an anti-cytokine antibody, and the other is cytocidal therapy using anticancer drugs or radiotherapy (Fig. 1) [18]. The goal of cytostatic therapy is to suppress cancer cell proliferation, migration, invasion and tumor angiogenesis, thus generating to a state of dormancy, while cytocidal therapy is aimed at a measurable reduction in tumor bulk. Regardless of cytostatic or cytocidal drugs, most of these drugs have been applied systemically via oral administration or intravenous injection. However, a complete cure has rarely been seen, and some severe adverse effects have been reported [19].

To achieve the markedly elevated pharmacological effect while minimizing systemic administration-associated toxic adverse effect, we have proposed and devised several trans-tissue and local delivery systems as shown below, all of which are processed to be tightly adhered or fixed on the resected tissues during surgery:

(1) System I: a drug-loaded photocured gelatinous tissue-adhesive gel (bioactive substance reser-

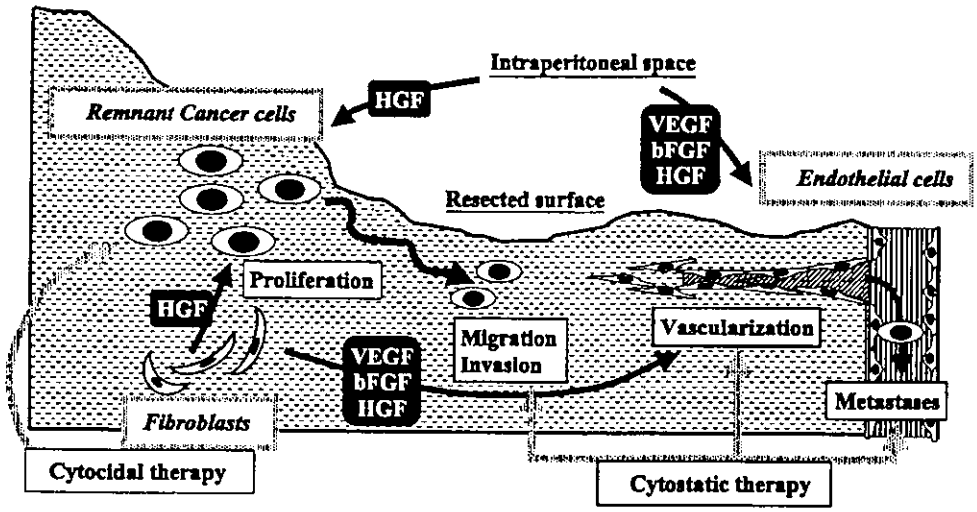

Fig. 1. Schematic of the progression of remnant cancer cells after surgery and relations with cytocidal and cytostatic therapies.

voir) that enables sustained release of a drug, protein, or gene-encoding adenovirus [20–22].

(2) System II: an anti-cytokine antibody-fixed photocured gelatinous, tissue-adhesive gel (cytokine barrier) that prevents cytokine permeation into the target tissue [23].

(3) System III: a gene-modified cell sheet that enables the sustained release of a very costly protein produced by gene-transduced cells [24].

(4) System IV: a percutaneous drug-delivery device that enables continuous drug infusion and easy detachment from the surgical site [25].

All the systems could be applicable for resected surfaces immediately after surgery (Fig. 2). The trans-tissue, local delivery systems devised have clear-cut advantages, including a high local concentration of drugs at the target tissue and a relatively low concentration at systemic organs, resulting in significant enhancement of the therapeutic effect of drugs and a marked reduction of systemic adverse effects.

In our studies [20–25], HGF antagonist, NK4, was used as a cytostatic drug. HGF plays an important role in tumor–stroma interaction and acts as a potent scattering factor by binding to c-Met

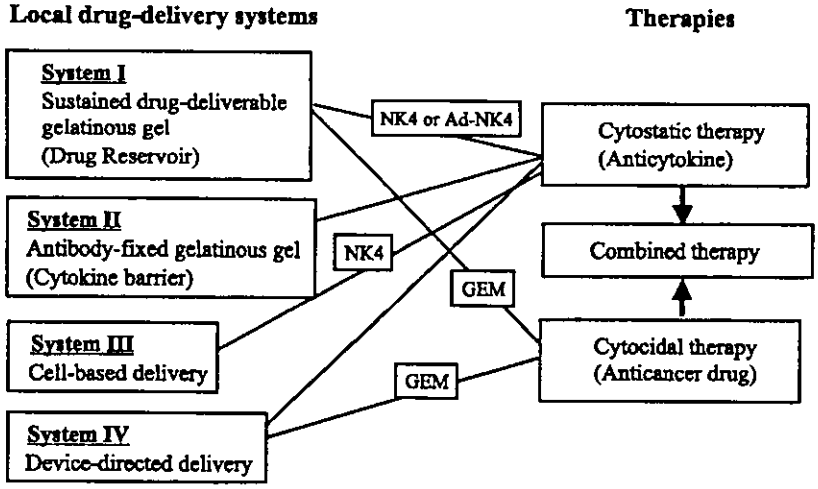

Fig. 2. Strategies for the prevention of local recurrence. NK4 is a cytostatic drug, which acts as a HGF antagonist and an angiogenic inhibitor. Gemcitabine (GEM) is a cytocidal drug, which acts as an antimetabolite [20–24].

receptor, which is frequently overexpressed in pancreatic cancers. NK4, composed of the N-terminal hairpin and four kringle domains of the α-subunit of HGF, binds to the c-Met receptor without tyrosine phosphorylation of c-Met, resulting in the inhibition of the mitogenic, motogenic and morphogenic activities of HGF [26–30]. Furthermore, NK4 acts as an angiogenic inhibitor, which inhibits the growth and migration of endothelial cells stimulated by VEGF, bFGF and HGF [31,32].

On the other hand, as a cytocidal drug, gemcitabine (2′,2′-difluorodeoxycitidine, GEM) was used. GEM, which inhibits DNA synthesis by the inhibition of ribonucleotide reductase and by its incorporation into DNA [33,34], is currently the most effective chemotherapeutic drug for pancreatic cancer. Several investigators reported that the cytocidal efficacy of GEM, which is an antimetabolite, increases with the exposure time [35–38].

This review article is a summary of our several years of efforts and attempts to overcome the recurrence of pancreatic cancer, and we outline our proposed strategies and discuss their promises and challenges in the clinical setting.

2. System I: drug-loaded gelatinous gel [20–22]

This system was developed to provide an in situ-formed locally deliverable gelatinous matrix that could adhere to the resected tissues, from which bioactive substances including drugs, proteins or gene-encoding adenoviruses can be sustainably released into the target tissue. To meet the desired performance in this particular application, the system should have the following characteristic features: (1) rapid sol-to-gel transformation by visible light photoirradiation, (2) strong tissue adhesivity, (3) ease of drug immobilization, (4) biodegradability and biosorption (5) minimal or very mild informatory reaction. To this end, photopolymerizable gelatin, which is partially derivatized with styrene groups in gelatin molecule (ST-gelatin; Fig. 3A), was used as an in situ gelable drug-loadable matrix. ST-gelatin was originally prepared at our laboratory as a visible light-induced photocurable tissue-adhesive glue, which prevented bleeding from arteries, indicating that such a glue inherently has a high tissue adhesivity, causes minimal inflammatory reaction and exhibits little sign of toxicity [39].

A viscous buffer solution composed of ST-gelatin, water-soluble carboxylated camphorquinone (visible light-induced radical generator used in clinical dental applications for many years), and the drug of interest was coated on resected tissues and photoirradiated with a visible light lamp (used in clinical dental applications), resulting in gel formation within 3 min of irradiation (Fig. 3B). The viscosity, in situ gelation time, drug-release rate, adhesive strength, and biodegradability were easily controlled by material (degree of derivatization of styrene groups in a gelatin molecule), formulation (concentrations of ST-gelatin and camphorquinone), and operation (photointensity and irradiation time) variables [20]. The general trend is that higher concentration of ST-gelatin, longer

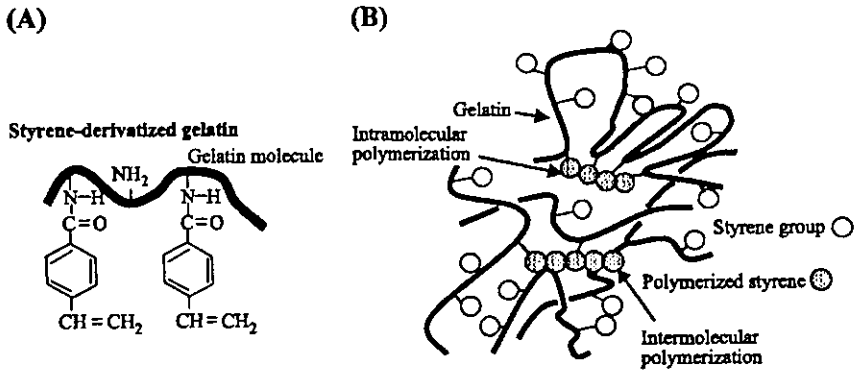

Fig. 3. Drug-loadable photocurable tissue-adhesive matrix. (A) Chemical structure of styrene-derivatized gelatin. (B) Photogelation by formation of cross-linked gelatin networks by the inter- and intra-molecular polymerizations of styrene groups in gelatin molecules.

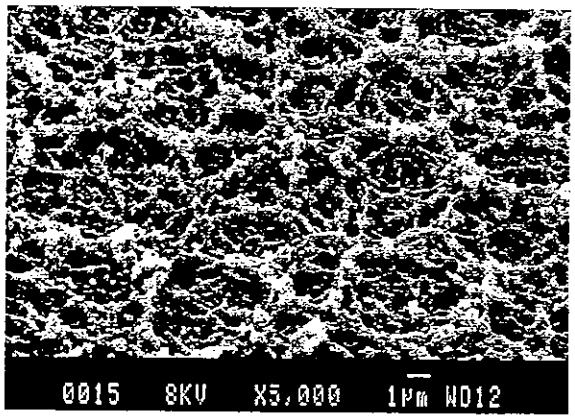

Fig. 4. Scanning electron micrograph of the beads-necklace type-surface of photocured ST-gelatin gel. Gelatin concentration: 30 wt.%. Bar: 1 μm [20].

photoirradiation time or higher photointensity produces a less water-swellable gel.

The formed gel consisted of supramolecular organization of polymerized gelatin with polymorphous nanostructures, which depends on the concentration of ST-gelatin and the degree of derivatization of styrene group in a gelatin molecule. The typical beaded necklace-type mesh appearance is shown in Fig. 4. The polymorphous nanostructured meshes or sheets of polymerized ST-gelatin are shown in Fig. 5. The general observation is that at low concentration of ST-gelatin, nanoparticles (diameter: approximately 100 nm) are adhered for each other to form continuous bead network with ample open-cell microvoids or channels (Fig. 5A1). Increased concentration of ST-gelatin produced beaded necklace-type mesh with a lesser degree of microvoids (Fig. 5A2). At high concentration, beads or necklace were fused to form a microporous continuous dense sheet (Fig. 5A3). In addition to the concentration of ST-gelatin, this tendency was enhanced with a lower degree of styrene derivatization (Fig. 5B). Such morphological features correlated well with the swellability of gel in water: Lower microvoid, lesser swellability. This in turn means that morphological features eventually determine the releasing profile of drug immobilized in a gel as shown below.

The typical time-dependent release profile of protein is a fast release in an early period, followed by reduced releasing characteristics (Fig. 6). The releasing rate of a proteinaceous drug was enhanced with a higher degree of swelling in water and with lower degree of derivatization of styrene in gelatin. The diffusion constants, calculated using Fick's second law, largely depended on the swellability of gels, which depends on the concentration of ST-gelatin (Fig. 7). The releasing period can be extended

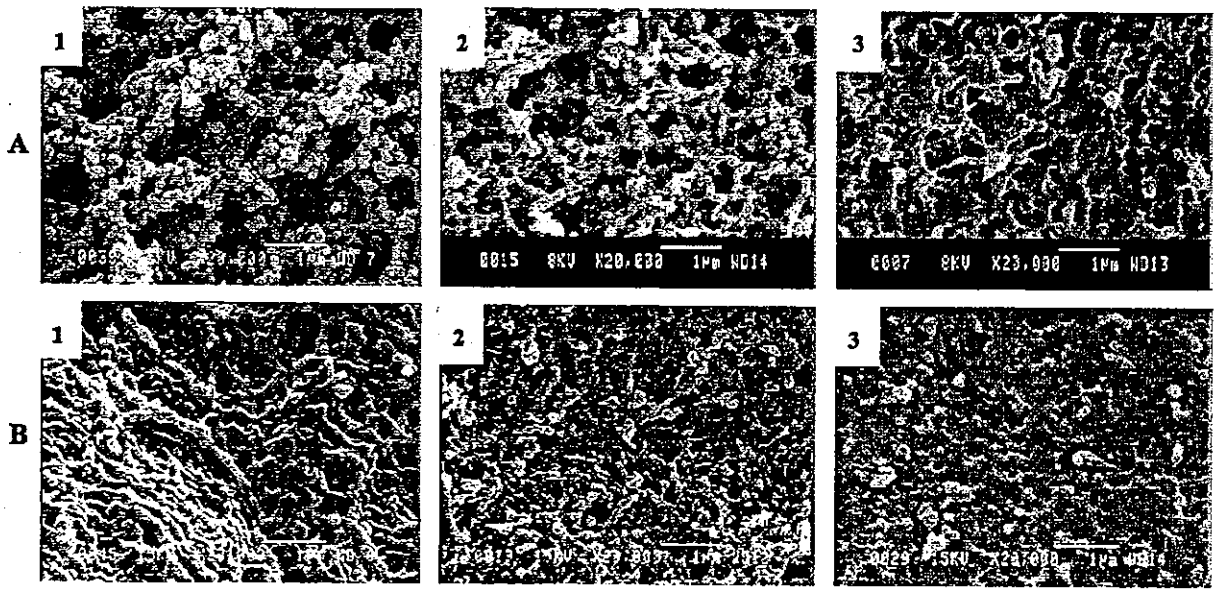

Fig. 5. Scanning electron micrographs of polymorphorous surfaces of photocured gelatins with variable concentration and variable styrene content in a gelatin molecule. Stryene content per molecule; 28.5 (A) and 22.4 (B). ST-gelatin content; 10 wt.% (1), 20 wt.% (2) and 40 wt.% (3). Bar: 1 μm.

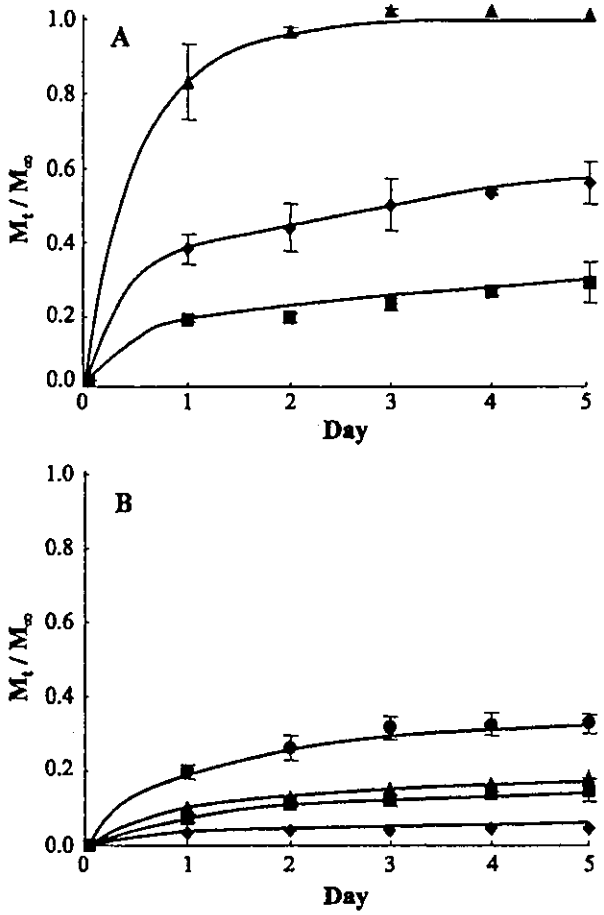

Fig. 6. Fraction release of rhodamine-albumin (r-Alb) as a function of time. Gel containing 10 wt.% (●), 20 wt.% (▲), 30 wt.% (■) and 50 wt.% (◆) of ST-gelatin of different contents of styrene per molecule (4.0 for A and 17.7 for B).

from days to several weeks, depending on the degree of photocuring or swellability of a formed gel. Fig. 8 shows the schematic of process of photogel formation and subsequent release of bioactive substances (A: drug, B: gene-encoding adenovirus) and experimental gel formation model using resected liver tissue (C). The followings are examples in System I loaded with bioactive substances.

2.1. NK4 [20]

The strategy for NK4 protein (MW; 64 000 g/mol) delivery is that an NK4-mixed ST-gelatin solution is photogelled on a target tissue where remnant cancer cells might remain, and NK4 released from the gel permeates gradually into the tissue, resulting in the suppression of cancer progression (Fig. 8A). The in vitro release profile of rhodamine-conjugated albumin (r-Alb, MW; 66 000 g/mol, used as a model protein of NK4) from ST-gelatin gel was characterized by an initial burst and subsequent gradual release over a prolonged period. In an in vivo experiment, 3 days after an r-Alb-loaded ST-gelatin solution was photogelled on the liver of a Wistar rat (Fig. 8C), r-Alb released from the gel remained in the liver from the surface to the deeper portions of the liver tissue. When NK4 is commercially manufactured at a low price, the prospective use of this system is very high. However, at present, NK4 is available only for experimental use in limited amounts so that it is doubtful that this system will be used in clinical situations in the near future.

2.2. NK4 gene-encoding adenovirus (Ad-NK4) [21]

Ad-NK4 is released from a photocured gelatinous gel formed on the tissue, and gradually permeates into the tissue, followed by transduction into various types of cells in the target tissue. Consequently, transduced cells produce NK4 (Fig. 8B). Although it is anticipated that the sustained release of an adenovirus might overcome the transient gene expression following adenoviral transduction, the amount of in vivo gene expression was substantially lower than that following simple injection of Ad-lacZ solution (Fig. 9A), probably because the adenoviral vector particles are too large to permeate the tissue via passive diffusion from the gel. In fact, our extensive study of gene transduction in rat's liver and muscle tissues showed

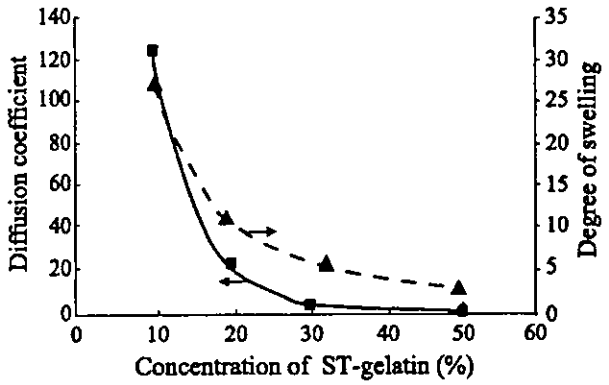

Fig. 7. Dependence of diffusion coefficient (■) and water swellability (▲) on concentration of ST-gelatin. Diffusion coefficient was obtained from the slope of the linear relation between M_t/M_∞ and $t^{1/2}$.

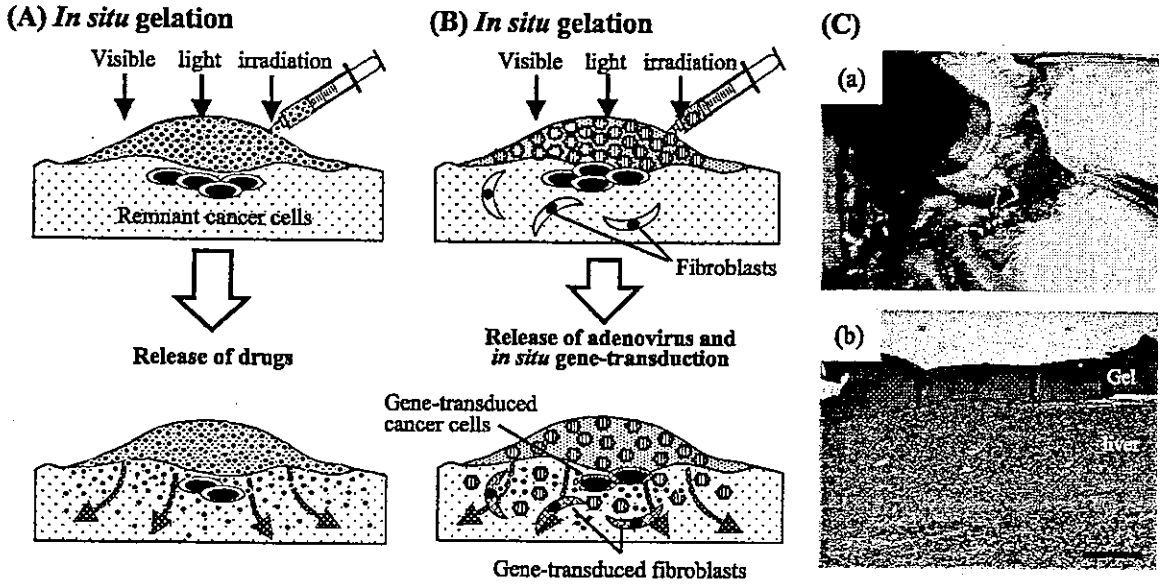

Fig. 8. Schematic of sustained drug-deliverable gelatinous gel (System I). (A) Local delivery of NK4 or Gemcitabine using photocurable gelatin. NK4- or Gemcitabine-loaded photocurable gelatin is coated on a tumor bed, and subsequently in situ photogelled under visible light irradiation. NK4 or Gemcitabine is released from the gel, and permeates into the tumor bed. (B) Local delivery of Ad-NK4 using photocurable gelatin. Ad-NK4-loaded photocurable gelatin is administered on a tumor bed, and subsequently in situ photogelled under visible light irradiation. Ad-NK4 is released from the gel, permeates into the tumor bed and transduces various cells around the tumor bed. Gene-transduced cells produce NK4. Irrespective of models, the inhibition of the progression of remnant cancer cells is expected. (C) In situ production of photocurable gelatin gel. (a) Procedure of visible-light irradiation of the aqueous gelatin solution on the liver surface. Gel formed on the liver surface. (b) Cross-sectional specimen (hematoxylin-and-eosin staining). Bar: 500 μm [20–22].

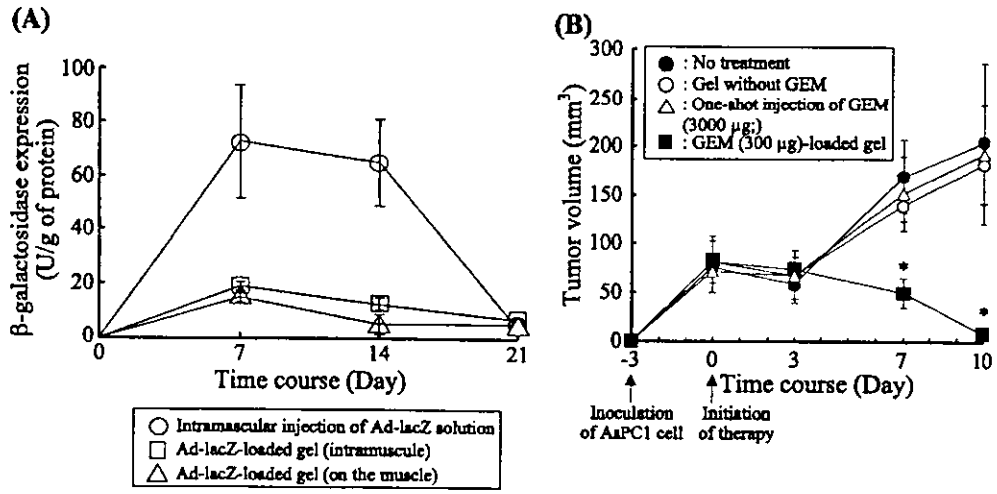

Fig. 9. (A) System I loaded with gene-encoding adenovirus. Time course of in vivo β-galactosidase expression in rat femoral muscle using Ad-lacZ-loaded gelatinous gel: One-shot intramuscular injection of Ad-lacZ solution (1.25×10^8 PFU/500 μl, ○), intramuscular injection of Ad-lacZ-loaded gel (1.25×10^8 PFU/500 μl, □), and covering on the muscle of Ad-lacZ-loaded gel (1.25×10^8 PFU/500 μl, △). The expression with the gel was lower than that of one-shot injection. Values are shown as means±S.D. (three mice/each group). (B) System I loaded with GEM. Effect of GEM-loaded photocured gelatinous gel on tumor growth of pancreatic cell line AsPC-1: no treatment (●), gel without GEM (○), one-shot injection of GEM (3000 μg; △), GEM (300 μg)-loaded gel (■). Values are shown as means±S.D. (10 mice/each group). The tumor volume with GEM-loaded gel was compared with that with the others (*$P<0.01$) [22].

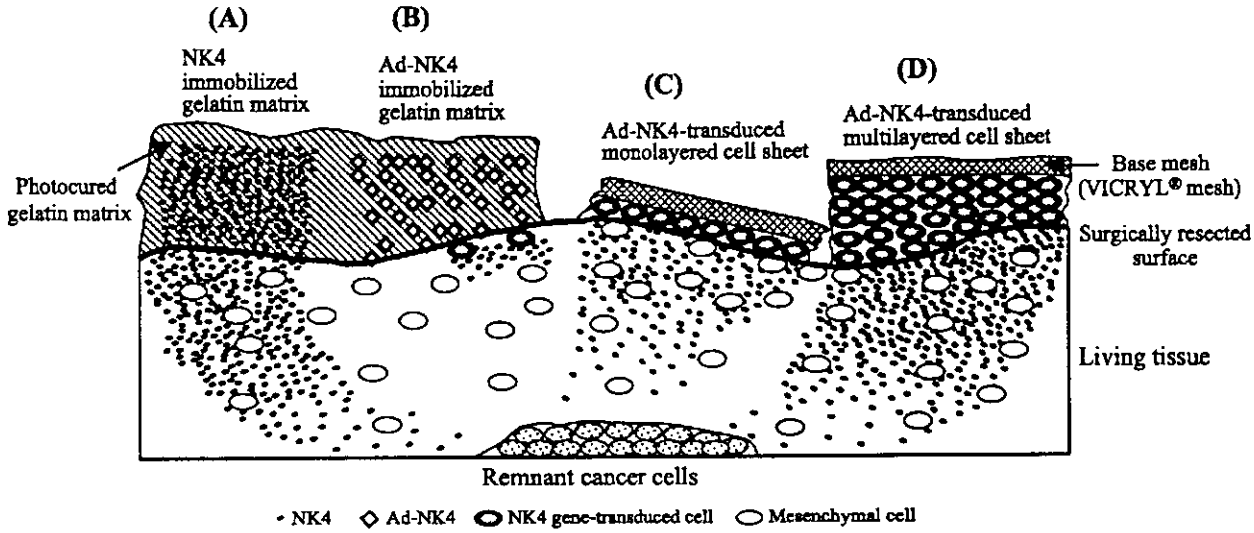

Fig. 10. Schematic of local protein delivery methods under development. (A) NK4-immobilized photocured gelatinous matrix. (B) Ad-NK4-immobilized photocured gelatinous matrix. (C) Ad-NK4-transduced monolayered cell sheet. (D) Ad-NK4-transduced multilayered cell sheet.

that the gene-transduced cell were found to be limited to on and just beneath the tissue surface. Therefore, it is highly anticipated that passive trans-tissue permeation of adenovirus, which is a giant macromolecules as compared with proteins, appears not to be effective for gene delivery [47,48]. Fig. 10 illustrates schematics of NK4- and Ad-NK4-immobilized gel layers and trans-tissue transport of NK4.

2.3. Gemcitabine (GEM) [22]

The in vitro release profile of GEM (MW; 299 g/mol) from a GEM-loaded ST-gelatin gel was characterized by an initial burst and subsequent gradual release over a prolonged period, similar to that of r-Alb from the gel. In an in vivo model using subcutaneous tumor-bearing athymic mice, rhodamine B (MW; 479 g/mol, used as a model drug of GEM) released from the ST-gelatin gel remained in the tumor at least for 10 days after photogelation on the inoculated tumor. When a GEM-loaded ST-gelatin was formed by injection, followed by subsequent photopolymerization on the inoculated tumor, the growth of the tumor was significantly suppressed without obvious adverse effects, as compared with simple GEM injection (Fig. 9B). Such suppression of tumor growth correlated with decreased cell proliferation and increased cell apoptosis in tumor cells, supported by PCNA (for proliferating cells) and TUNEL (for apoptosed cells) staining. Therefore, this strategy is considered to be highly prospective. A possible disadvantage of this system is difficulty of realization of appropriate drug-releasing profile: an adverse effect resulting from an "overdose", weak therapeutic effect due to too low dose and short releasing period due to no recharging function.

3. System II: antibody-fixed gelatinous gel (cytokine barrier) [23]

A styrene-derivatized antibody (ST-Ab), prepared with minimal affinity loss, was photocopolymerized with ST-gelatin to produce a tissue-adhesive, in situ-formed co-gel of ST-gelatin and ST-Ab, which is designed to act as a cytokine scavenger, neutralizer or barrier. A double-chamber invasion assay using an anti-HGF antibody showed that the co-gel prevented the HGF-dependent invasion of pancreatic cancer cells. On the basis of such an experimental result, when a co-gel of ST-gelatin and anti-cytokine ST-Ab is produced on a target tissue, it is anticipated that it would work well as a cytokine barrier to prevent the permeation of cytokines into the target tissue (Fig. 11A and C). Such a cytokine barrier based on an anti-cytokine fixed gel might not affect distant sites, because the antibodies were fixed in the gel, resulting in little release of the antibodies. On the other hand,

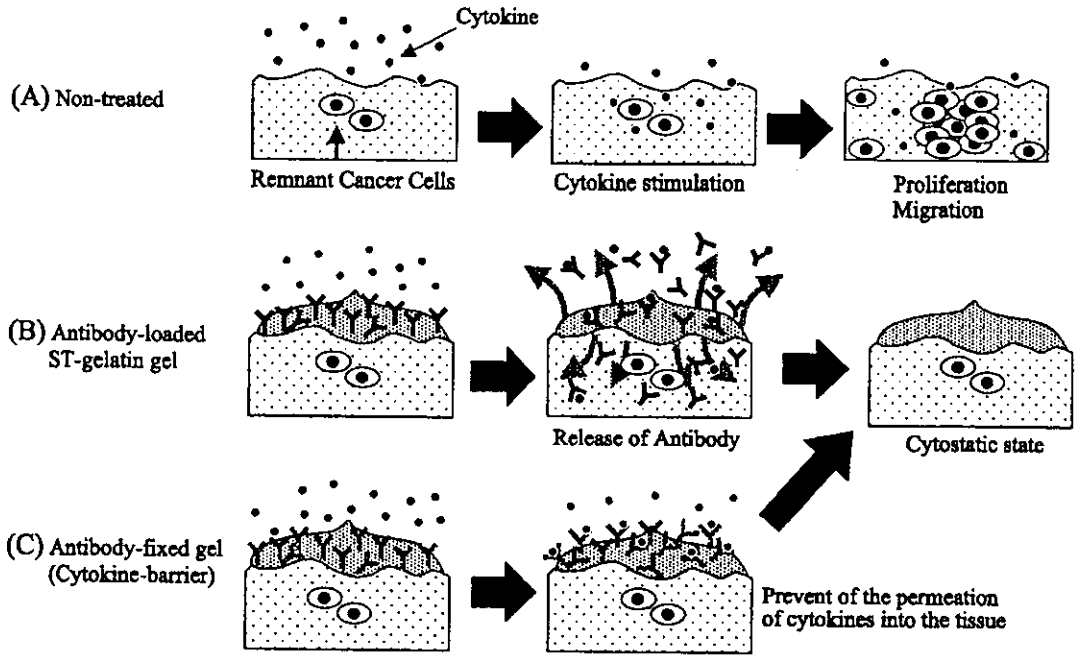

Fig. 11. Schematic of the strategy of a cytokine barrier (System II). (A) Various cytokines, produced in the intraperitoneal space during wound healing after abdominal surgery, affect remnant cancer cells in surgically resected tissues. (B) Antibody-loaded ST-gelatin gel on resected tissues. Antibodies are released from the gel, neutralize cytokines in and out of a gel, and prevent the effect of cytokines on remnant cancer cells. (C) The co-gel prepared by copolymerization of ST-gelatin and anti-cytokine ST-antibody on resected tissues. Antibodies fixed in a gel neutralize cytokines, which permeated into a gel, thereby preventing the permeation and penetration of cytokines into resected tissues [23].

when an antibody-mixed ST-gelatin solution was photogelled on a target tissue, antibodies were released from the gel and neutralized the cytokines as described above. The prevention of the permeation of cytokine into the tissue apparently results in a cytostatic state (Fig. 11). The co-gel could also be used as a drug-release matrix, from which GEM, NK4, or cytokine antibody could be released.

4. System III: cell-based delivery [24]

A hybrid tissue composed of ex vivo *NK4* gene-transduced cells was prepared for the in situ production of NK4 on a target tissue (Figs. 10C and 12). The cell source used was oral mucosal epithelial cells (OMECs), which were found to be suited to NK4 delivery because they do not secrete HGF and are easy to harvest from patients, and have reasonably high proliferation potential. OMECs were seeded on a collagen mesh-overlayered, biodegradable VICRYL® mesh, and subsequently transduced using Ad-NK4 to produce the hybrid tissue composed of NK4 gene-transduced OMECs (OMEC sheet, Fig. 12). Heterotopically implanted gene-transduced OMECs remained for at least 10 days while gradually decreasing. In an in vivo model using subcutaneous tumor-bearing nude mice, NK4 gene-transduced OMEC sheets implanted on the tumor inhibited both tumor angiogenesis (Fig. 13B) and tumor growth (Fig. 13A). Thus, it is expected that this system, developed fully using combined tissue-engineering and genetic-engineering techniques, may have great potential as a protein delivery system to target tissue at the clinical situations. The shortcomings of a prototype technology, such as the low level and short period of NK4 production, may be overcome by high density seeding of gene-transduced cells, e.g., multilayering on a microporous matrix as schematically shown in Fig. 10D. It is highly envisaged that the combination of a high cell seeding and more powerful vector enabling longer term NK4 secretion, such as retrovirus vectors, overcome the shortcomings of the prototype cell-sheet device in

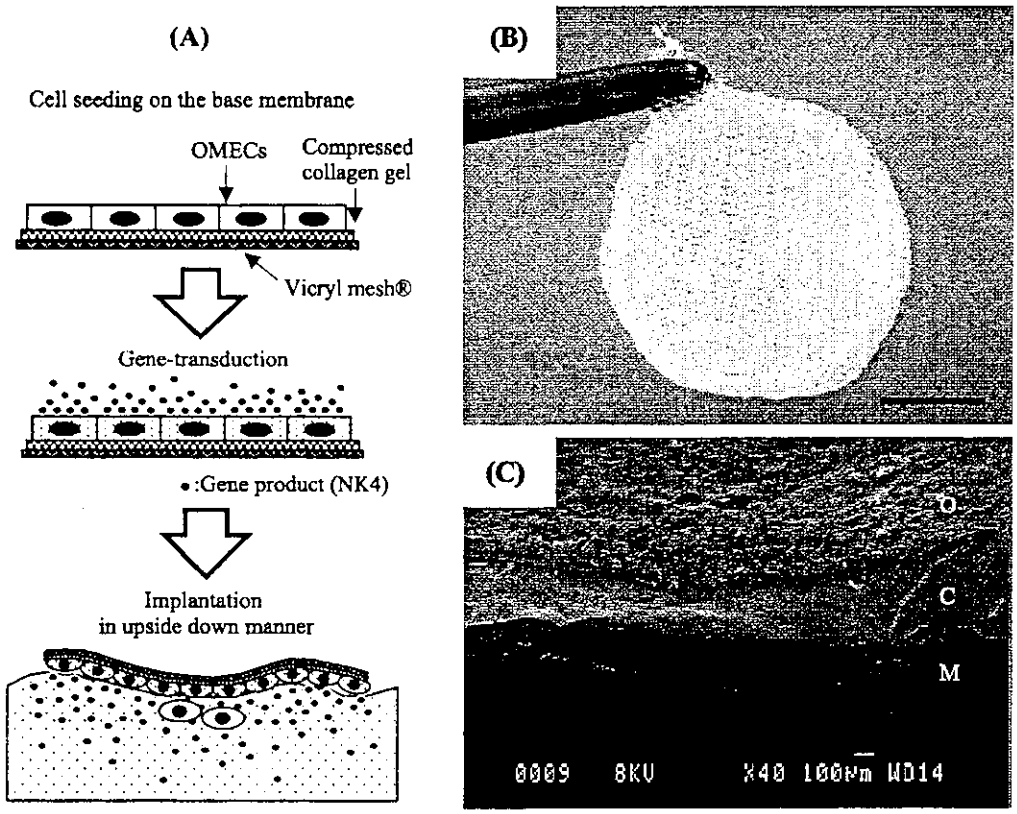

Fig. 12. System III: Cell-based delivery. (A) Schematic of gene-transduced oral mucosal epithelial cell (OMEC) sheet and the method of implantation. (B) Gross appearance of OMEC sheet. (C) Scanning electron microscopy of OMEC sheet. O, OMECs; C, collagen mesh; M, biodegradable VICRYL® mesh. Bar: 100 μm [24].

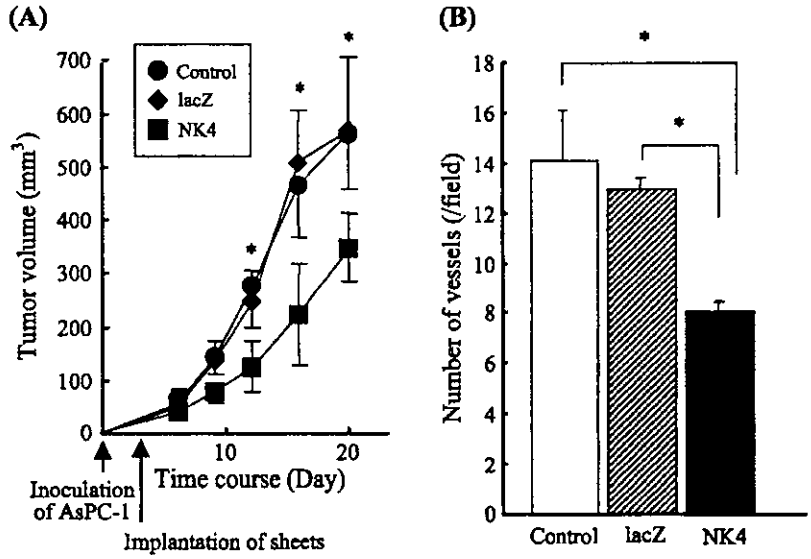

Fig. 13. Effect of NK4 gene-transduced OMEC sheet on tumor growth. Three days after cancer cell (AsPC-1) injection, tumors were covered with lacZ or NK4 gene transduced OMEC sheet. In the control group, mice were not treated. (A) Development of tumor arising from AsPC-1 cells. Values are expressed as means±S.D. (n=5, *P<0.05). (B) The number of vessels of tumors of each group. Values are expressed as means±S.D. (*P<0.05) [24].

this study. Further studies are required to increase the amount and period of in situ production of NK4.

5. System IV: device-directed delivery [25]

A rechargeable drug infusion device, which can be attached to the resected site and from which a drug is infused into the resected site, was devised (Fig. 14A). The device is composed of an elastomeric pouch (made of segmented polyurethane; SPU) having a microporous film on one side and a port connected to an elastomeric tube. The device connected to the tube guided to the extracorporeal portion permits continuous administration and recharge from the extracorporeal tube. After a few to several weeks of infusion, the device is easily removed due to the use of biodegradable sutures. The pouch is very thin (approximately 100 μm in thickness) and flexible (note that SPU, used for a diagram of artificial hearts, has proven flexibility and durability), so that the mechanically folded device is removed percutaneously through a small-sized incision upon pull-out. The prototype was fabricated with segmented polyurethane, which permits tight attachment to resected tissues using biodegradable sutures, and has multi-micropores on the side of delivery, created by a laser ablation technique coupled with computer-aided design and manufacture (Fig. 14B). In an in vivo experiment using subcutaneous tumor-bearing athymic mice, continuous infusion of GEM (150 μg/body/for 1week) from the device attached to the tumor-bearing tissue markedly suppressed tumor growth (Fig. 14C) [25]. This device, which is attached to tissue with commercially available, biodegradable sutures, can be removed easily when an adverse effect occurs or when therapy becomes unnecessary. Efforts to translate this system to the clinical situation are now underway.

6. Perspectives

The major causes of the death of patients who have undergone resection for pancreatic cancer are local recurrence and hepatic metastasis. Regarding hepatic metastasis, local chemotherapy via blood vessels has

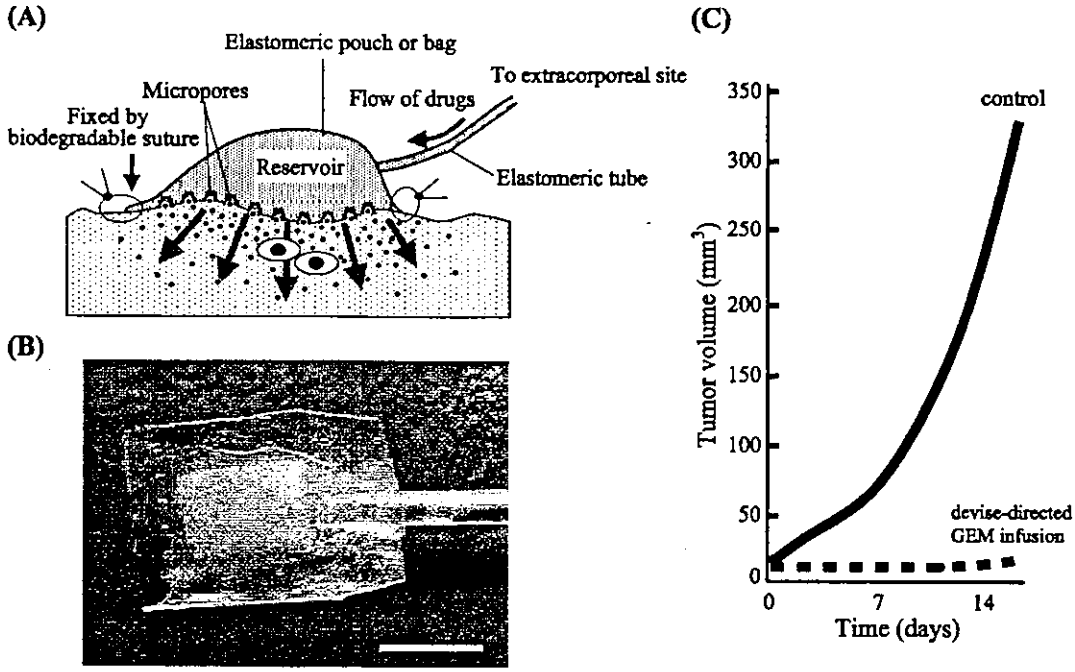

Fig. 14. System IV: Device-directed therapy. (A) Schematic of local drug delivery device. The pouch of the device is fixed on the target tissue by biodegradable sutures. Elastomeric tube connected to the pouch is guided to the extracorporeal site, which enables recharge of drugs and easy removal of the device. (B) The prototype device made by micropored segmented polyurethane. Bar: 5 mm [25]. (C) The growth of subcutaneously inoculated pancreatic cancer cell (AsPC-1). The initial tumor volume was about 20 mm^3.

been reported to reduce the occurrence of hepatic metastasis, resulting in an improvement in survival rate [40–43]. On the other hand, although several therapeutic strategies to prevent local recurrence, such as intraoperative radiotherapy, systemic chemotherapy and their combinations, have been attempted, the effect on survival rate is still under debate [9–11]. Therefore, a more effective therapeutic modality is awaited. Although a drug-delivery system used in the preclinical and clinical treatments for a variety of cancers has been reported [44–46], there have been no experimental or clinical attempts to develop a local delivery system constructed in situ on resected tissues to date. Our concept is that such a trans-tissue, local delivery system should be constructed shortly after surgical resection to minimize tumor progression caused by potent autocrine cytokines using cytostatic drugs and to enhance the cytotoxic effects of cytocidal drugs in the target tissue at very low dosage but by continuous drug exposure. For the last several years, we have been developing various new therapeutic procedures based on local drug-delivery systems as mentioned above [20–25].

Irrespective of the systems, such as a photocurable gelatinous gel (Systems I and II), a gene-transduced cell sheet (System III), and a newly devised drug-delivery device (System IV), all the therapeutic devices or materials described here can be tightly attached to the wet and uneven resected surfaces immediately after resection during surgery, and permit the local, trans-tissue delivery of various types of bioactive substances, such as anti-cancer drugs, proteins and adenoviruses, or preventing the permeation of potent tumor-progressing cytokines to the target tissue. As for the in situ gellable tissue-adhesive gel, we used photocurable gelatin which cure via visible light-induced radical polymerization of styrene group multiply derivatized on a gelatin molecule. This is originally designed to use as a hemostatic glue for surgically injured arteries during cardiovascular surgery. The rapid sol-to-gel transformation and strong tissue adhesivity withstanding against continuously loaded pulsatile stress are found to be very advantageous for trans-tissue drug delivery. Other potential candidate polymers, which meet the requirements for this particular application, may be thermoresponsible polymers which enables the sol-to-gel transformation at physiological temperature. These polymers include poly(*N*-isopropylacrylamide) or poly(ethylene glycol)–poly(propylene glycol) triblock copolymer. However, tissue adhesivity of these gels is eventually very poor due to nonionic hydrogel. In Systems I, II and IV, both cytostatic and cytocidal drugs could be delivered simultaneously, so that a more powerful synergistic effect may be expected. Caution must be paid for co-drug delivery which may cause unexpected adverse effect.

When these strategies or their combinations are applied in clinical situations as an adjuvant therapy for pancreatic cancer after thorough examination, the authors strongly envisage that the incidence of local recurrence could be reduced, hopefully resulting in a marked improvement in survival rate after surgery. To this end, research is now planned to translate these new strategic therapies in a clinical setting.

Acknowledgments

This study is financially supported by Promotion Fundamental Studies in Health Science of the Organization for Pharmaceutical Safety and Research (OPSR, contract grant number: 97-15) and Grant-in-Aid for Scientific Research from Ministry of Education, Culture, Sports, Science, and Technology of Japan (contract grant number: A2-12358017 and B2-12470277).

References

[1] T. Nakagohri, T. Kinoshita, M. Konishi, K. Inoue, S. Takahashi, Survival benefits of portal vein resection for pancreatic cancer, Am. J. Surg. 186 (2003) 149–153.
[2] T. Nagakawa, M. Nagamori, F. Futakami, Y. Tsukioka, M. Kayahara, T. Ohta, K. Ueno, I. Miyazaki, Results of extensive surgery for pancreatic carcinoma, Cancer 77 (1996) 640–645.
[3] M. Trede, G. Schwall, H.D. Saeger, Survival after pancreatoduodenectomy. 118 consecutive resections without an operative mortality, Ann. Surg. 211 (1990) 447–458.
[4] J.L. Cameron, D.W. Crist, J.V. Sitzmann, R.H. Hruban, J.K. Boitnott, A.J. Seidler, J. Coleman, Factors influencing survival after pancreaticoduodenectomy for pancreatic cancer, Am. J. Surg. 161 (1991) 120–124 (discussion 124–125).
[5] C. Sperti, C. Pasquali, A. Piccoli, S. Pedrazzoli, Recurrence after resection for ductal adenocarcinoma of the pancreas, World J. Surg. 21 (1997) 195–200.

[6] M. Kayahara, T. Nagakawa, K. Ueno, T. Ohta, T. Takeda, I. Miyazaki, An evaluation of radical resection for pancreatic cancer based on the mode of recurrence as determined by autopsy and diagnostic imaging, Cancer 72 (1993) 2118–2123.
[7] J.F. Griffin, S.R. Smalley, W. Jewell, J.C. Paradelo, R.D. Reymond, R.E. Hassanein, R.G. Evans, Patterns of failure after curative resection of pancreatic carcinoma, Cancer 66 (1990) 56–61.
[8] J. Westerdahl, A. Andren-Sandberg, I. Ihse, Recurrence of exocrine pancreatic cancer—local or hepatic? Hepatogastroenterology 40 (1993) 384–387.
[9] J.A. Cienfuegos, F.A. Manuel, Analysis of intraoperative radiotherapy for pancreatic carcinoma, Eur. J. Surg. Oncol. 26 (Suppl. A) (2000) S13–S15.
[10] W.F. Sindelar, T.J. Kinsella, Studies of intraoperative radiotherapy in carcinoma of the pancreas, Ann. Oncol. 10 (Suppl. 4) (1999) 226–230.
[11] A. Zerbi, V. Fossati, D. Parolini, M. Carlucci, G. Balzano, G. Bordogna, C. Staudacher, V. Di Carlo, Intraoperative radiation therapy adjuvant to resection in the treatment of pancreatic cancer, Cancer 73 (1994) 2930–2935.
[12] R.K. Jain, Barriers to drug delivery in solid tumors, Sci. Am. 271 (1994) 58–65.
[13] I.F. Tannock, Tumor physiology and drug resistance, Cancer Metastasis Rev. 20 (2001) 123–132.
[14] S.O. Hofer, G. Molema, R.A. Hermens, H.J. Wanebo, J.S. Reichner, H.J. Hoekstra, The effect of surgical wounding on tumour development, Eur. J. Surg. Oncol. 25 (1999) 231–243.
[15] S.O. Hofer, D. Shrayer, J.S. Reichner, H.J. Hoekstra, H.J. Wanebo, Wound-induced tumor progression: a probable role in recurrence after tumor resection, Arch. Surg. 133 (1998) 383–389.
[16] D.G. Baker, T.M. Masterson, R. Pace, W.C. Constable, H. Wanebo, The influence of the surgical wound on local tumor recurrence, Surgery 106 (1989) 525–532.
[17] M.N. Svendsen, K. Werther, H.J. Nielsen, P.E. Kristjansen, VEGF and tumour angiogenesis. Impact of surgery, wound healing, inflammation and blood transfusion, Scand. J. Gastroenterol. 37 (2002) 373–379.
[18] E.C. Kohn, L.A. Liotta, Molecular insights into cancer invasion: strategies for prevention and intervention, Cancer Res. 55 (1995) 1856–1862.
[19] A. Inoue, Y. Saijo, M. Maemondo, K. Gomi, Y. Tokue, Y. Kimura, M. Ebina, T. Kikuchi, T. Moriya, T. Nukiwa, Severe acute interstitial pneumonia and gefitinib, Lancet 361 (2003) 137–139.
[20] H. Okino, Y. Nakayama, M. Tanaka, T. Matsuda, In situ hydrogelation of photocurable gelatin and drug release, J. Biomed. Mater. Res. 59 (2002) 233–245.
[21] H. Okino, T. Manabe, M. Tanaka, T. Matsuda, Novel therapeutic strategy for prevention of malignant tumor recurrence after surgery: local delivery and prolonged release of adenovirus immobilized in photocured, tissue-adhesive gelatinous matrix, J. Biomed. Mater. Res. 66A (2003) 643–651.
[22] H. Okino, R. Maeyama, T. Manabe, T. Matsuda, M. Tanaka, Trans-tissue, sustained release of gemcitabine from photocured gelatin gel inhibits the growth of heterotopic human pancreatic tumor in nude mice, Clin. Cancer Res. 9 (2003) 5786–5793.
[23] T. Manabe, H. Okino, M. Tanaka, T. Matsuda, In situ-formed, tissue-adhesive co-gel composed of styrenated gelatin and styrenated antibody: potential use for local anti-cytokine antibody therapy on surgically resected tissues, Biomaterials 25 (2004) 5867–5873.
[24] T. Manabe, K. Mizumoto, E. Nagai, K. Matsumoto, T. Nakamura, T. Nukiwa, M. Tanaka, T. Matsuda, Cell-based protein delivery system for the inhibition of the growth of pancreatic cancer: NK4 gene-transduced oral mucosal epithelial cell sheet, Clin. Cancer Res. 9 (2003) 3158–3166.
[25] T. Manabe, H. Okino, R. Maeyama, M. Tanaka, T. Matsuda, The new infusion device for trans-tissue, sustained local delivery of Gemcitabine: potential use for the suppression of local recurrence of pancreatic cancer, J. Biomed. Mater. Res. (in press).
[26] W. Jiang, S. Hiscox, K. Matsumoto, T. Nakamura, Hepatocyte growth factor/scatter factor, its molecular, cellular and clinical implications in cancer, Crit. Rev. Oncol. Hematol. 29 (1999) 209–248.
[27] K. Matsumoto, K. Date, H. Ohmichi, T. Nakamura, Hepatocyte growth factor in lung morphogenesis and tumor invasion: role as a mediator in epithelium–mesenchyme and tumor–stroma interactions, Cancer Chemother. Pharmacol. 38 (1996) S42–S47.
[28] K. Date, K. Matsumoto, K. Kuba, H. Shimura, M. Tanaka, T. Nakamura, Inhibition of tumor growth and invasion by a four-kringle antagonist (HGF/NK4) for hepatocyte growth factor, Oncogene 17 (1998) 3045–3054.
[29] K. Date, K. Matsumoto, H. Shimura, T. Tanaka, T. Nakamura, HGF/NK4 is a specific antagonist for pleiotrophic actions of hepatocyte growth factor, FEBS Lett. 420 (1997) 1–6.
[30] N. Maehara, K. Matsumoto, K. Kuba, K. Mizumoto, M. Tanaka, T. Nakamura, NK4, a four-kringle antagonist of HGF, inhibits spreading and invasion of human pancreatic cancer cells, Br. J. Cancer 84 (2001) 864–873.
[31] K. Kuba, K. Matsumoto, K. Ohnishi, T. Shiratsuchi, M. Tanaka, T. Nakamura, Kringle 1–4 of hepatocyte growth factor inhibits proliferation and migration of human microvascular endothelial cells, Biochem. Biophys. Res. Commun. 279 (2000) 846–852.
[32] K. Kuba, K. Matsumoto, K. Date, H. Shimura, M. Tanaka, T. Nakamura, HGF/NK4, a four-kringle antagonist of hepatocyte growth factor, is an angiogenesis inhibitor that suppresses tumor growth and metastasis in mice, Cancer Res. 60 (2000) 6737–6743.
[33] L.W. Hertel, G.B. Boder, J.S. Kroin, S.M. Rinzel, G.A. Poore, G.C. Todd, G.B. Grindey, Evaluation of the antitumor activity of gemcitabine (2′,2′-difluoro-2′-deoxycytidine), Cancer Res. 50 (1990) 4417–4422.
[34] R.L. Merriman, L.W. Hertel, R.M. Schultz, P.J. Houghton, J.A. Houghton, P.G. Rutherford, L.R. Tanzer, G.B. Boder, G.B. Grindey, Comparison of the antitumor activity of gemcitabine and ara-C in a panel of human breast, colon, lung and pancreatic xenograft models, Invest. New Drugs 14 (1996) 243–247.

[35] V.W. Ruiz van Haperen, G. Veerman, P. Noordhuis, J.B. Vermorken, G.J. Peters, Concentration and time dependent growth inhibition and metabolism in vitro by 2′,2′-difluorodeoxycytidine (gemcitabine), Adv. Exp. Med. Biol. 309A (1991) 57–60.

[36] V.W. Ruiz van Haperen, G. Veerman, E. Boven, P. Noordhuis, J.B. Vermorken, G.J. Peters, Schedule dependence of sensitivity to 2′,2′-difluorodeoxycytidine (Gemcitabine) in relation to accumulation and retention of its triphosphate in solid tumour cell lines and solid tumours, Biochem. Pharmacol. 48 (1994) 1327–1339.

[37] G. Veerman, V.W. Ruiz van Haperen, J.B. Vermorken, P. Noordhuis, B.J. Braakhuis, H.M. Pinedo, G.J. Peters, Antitumor activity of prolonged as compared with bolus administration of 2′,2′-difluorodeoxycytidine in vivo against murine colon tumors, Cancer Chemother. Pharmacol. 38 (1996) 335–342.

[38] M. Kornmann, U. Butzer, J. Blatter, H.G. Beger, K.H. Link, Pre-clinical evaluation of the activity of gemcitabine as a basis for regional chemotherapy of pancreatic and colorectal cancer, Eur. J. Surg. Oncol. 26 (2000) 583–587.

[39] C. Li, T. Sajili, Y. Nakayama, M. Fukui, T. Matsuda, Novel visible-light-induced photocurable tissue adhesive composed of multiply styrene-derivatized gelatin and poly(ethylene glycol) diacrylate, J. Biomed. Mater. Res. 66B (2003) 439–446.

[40] O. Ishikawa, H. Ohigashi, Y. Sasaki, H. Furukawa, T. Kabuto, M. Kameyama, S. Nakamori, M. Hiratsuka, S. Imaoka, Liver perfusion chemotherapy via both the hepatic artery and portal vein to prevent hepatic metastasis after extended pancreatectomy for adenocarcinoma of the pancreas, Am. J. Surg. 168 (1994) 361–364.

[41] O. Ishikawa, H. Ohigashi, S. Imaoka, Y. Sasaki, M. Kameyama, S. Nakamori, T. Kabuto, H. Furukawa, Regional chemotherapy to prevent hepatic metastasis after resection of pancreatic cancer, Hepatogastroenterology 44 (1997) 1541–1546.

[42] H.G. Beger, F. Gansauge, M.W. Buchler, K.H. Link, Intra-arterial adjuvant chemotherapy after pancreaticoduodenectomy for pancreatic cancer: significant reduction in occurrence of liver metastasis, World J. Surg. 23 (1999) 946–949.

[43] H.G. Beger, K.H. Link, F. Gansauge, Adjuvant regional chemotherapy in advanced pancreatic cancer: results of a prospective study, Hepatogastroenterology 45 (1998) 638–643.

[44] C.M. Lee, T. Tanaka, T. Murai, M. Kondo, J. Kimura, W. Su, T. Kitagawa, T. Ito, H. Matsuda, M. Miyasaka, Novel chondroitin sulfate-binding cationic liposomes loaded with cisplatin efficiently suppress the local growth and liver metastasis of tumor cells in vivo, Cancer Res. 62 (2002) 4282–4288.

[45] T. Tamura, F. Fujita, M. Tanimoto, M. Koike, A. Suzuki, M. Fujita, Y. Horikiri, Y. Sakamoto, T. Suzuki, H. Yoshino, Antitumor effect of intraperitoneal administration of cisplatin-loaded microspheres to human tumor xenografted nude mice, J. Control. Release 80 (2002) 295–307.

[46] M. Lohr, F. Hummel, G. Faulmann, J. Ringel, R. Saller, J. Hain, W.H. Gunzburg, B. Salmons, Microencapsulated, CYP2B1-transfected cells activating ifosfamide at the site of the tumor: the magic bullets of the 21st century, Cancer Chemother. Pharmacol. 2002 (Suppl. 1) (2002) S21–S24.

[47] R.K. Jain, Barriers to drug delivery in solid tumors, Sci. Am. 271 (1) (1994) 42–49.

[48] R.K. Jain, Delivery of molecular medicine to solid tumors: lesson from in vivo imaging of gene expression and function, J. Control. Release 74 (1–3) (2001) 7–25.

Confocal imaging of biofilm formation process using fluoroprobed *Escherichia coli* and fluoro-stained exopolysaccharide

Ryo Maeyama,[1,2] Yoshimitsu Mizunoe,[3] James M. Anderson,[4] Masao Tanaka,[2] Takehisa Matsuda[1]
[1]*Department of Biomedical Engineering, Faculty of Medical Sciences, Kyushu University, Maidashi, Fukuoka 812-8582, Japan*
[2]*Department of Surgery and Oncology, Faculty of Medical Sciences, Kyushu University, Maidashi, Fukuoka 812-8582, Japan*
[3]*Department of Bacteriology, Faculty of Medical Sciences, Kyushu University, Maidashi, Fukuoka 812-8582, Japan*
[4]*Department of Pathology, Case Western Reserve University, 2085, Adelbert Road, Cleveland, Ohio 44106-4907*

Received 5 March 2004; revised 17 March 2004; accepted 19 March 2004
Published online 4 June 2004 in Wiley InterScience (www.interscience.wiley.com). DOI: 10.1002/jbm.a.30077

Abstract: We developed a novel method of evaluating biofilm architecture on a synthetic material using green fluorescent protein-expressing *Escherichia coli* and red fluorescence staining of exopolysaccharides. Confocal laser scanning microscopy observation revealed the time course of the change in the *in situ* three-dimensional structural features of biofilm on a polyurethane film without structural destruction: initially adhered cells are grown to form cellular aggregates and secrete exopolysaccharides. These cells were spottily distributed on the surface at an early incubation time but fused to form a vertically grown biofilm with incubation time. Fluorescence intensity, which is a measure of the number of cells, determined using a fluorometer and biofilm thickness determined from confocal laser scanning microscopy vertical images were found to be effective for quantification of time-dependent growth of biofilms. The curli (surface-located fibers specifically binding to fibronectin and laminin)–producing *Escherichia coli* strain, YMel, significantly proliferated on fibronectin-coated polyurethane, whereas the curli-deficient isogenic mutant, YMel-1, did not. The understanding of biofilm architecture in molecular and morphological events and new fluorescence microscopic techniques may help in the logical surface design of biomaterials with a high antibacterial potential. © 2004 Wiley Periodicals, Inc. J Biomed Mater Res 70A: 274–282, 2004

Key words: biofilm; green fluorescent protein; confocal laser scanning microscopy; *Escherichia coli*; curli

INTRODUCTION

The biomass of bacteria and extracellular materials including exopolysaccharides (EPS) that accumulate on synthetic substrates is called a biofilm.[1,2] Once a biofilm is formed on artificial implants in the body, serious, often life-threatening events or situations such as "septic shock," defined as a systemic response to infection, occur, which cannot be managed by antimicrobial drug administration due to a high level of resistance to drug diffusion into the well-stabilized biofilm bioarchitecture.[3] Implanted artificial prostheses, which are often associated with biomaterial-based biofilms, include cardiovascular implants, orthopedic replacements, intraocular implants, and intravascular catheters. Biliary stents and urinary catheters are often occluded by biofilms of *Escherichia coli*, resulting in complications in patients.[4] For cardiovascular implants, a second surgery to replace a bacterial-infected implant with a new one is often necessary.

The microbial colonization, and the nature and architecture of biofilms on synthetic polymers have been studied over a few decades. Previous studies have revealed various aspects of biofilms qualitatively as well as quantitatively, particularly focusing on adhered and proliferated cells by microscopy, plate counting, or dye-staining technique.[5–8] Electron microscopy has been used to observe the three-dimen-

Correspondence to: T. Matsuda; e-mail: matsuda@med.kyushu-u.ac.jp
Contract grant sponsor: Ministry of Health, Labour and Welfare (MHLW) of Japan, Grant-in-Aid for Scientific Research
Contract grant sponsor: Ministry of Education, Culture, Sports, Science, and Technology (MEXT) of Japan, Grant-in-Aid for Scientific Research and for the Creation of Innovations through Business-Academic-Public Sector Cooperation
Contract grant sponsor: NIH/NIBIB; contract grant number: EB-00279

sional (3D) structural features of biofilms.[9] However, this method often destroys biofilms because of complicated fixation procedures such as dehydration and fails to show an "as-is" structure.[10] Therefore, the formation of an as-is 3D structure of a biofilm of *E. coli* on synthetic polymers has not yet been fully understood.

Confocal laser scanning microscopy (CLSM) enables the high-resolution fluorescence imaging and deep optical sectioning of biological structures with negligible background interface. Additionally, CLSM enables a biofilm to be observed under hydrated conditions, thus maintaining an as-is structure without structure destruction.[11] When combined with fluorescent probes, CLSM can be effectively used for the visualization of biofilm components. In recent years, green fluorescent protein (GFP) from jellyfish *Aequorea victoria* has emerged as an *in situ* marker of living cells. EPS, which are produced by *E. coli* and which serve as structural anchors for bacterial cells in biofilms, can be specifically stained with a fluorescent dye, rhodamine-labeled lectin.[12,13] The co-use of GFP-expressing *E. coli* and rhodamine-labeled lectin under CLSM enables us to obtain in-depth information on the distribution state of the bacterial and EPS components of 3D biofilms.

The objective of this study was to perform an *in situ* visualization of the 3D structure of *E. coli*–based biofilm on polyurethane (PU) films. *In situ* monitoring using the CLSM technique enabled us to analyze the time-dependent construction of 3D-structured biofilms on a synthetic polymer. Two *E. coli* strains, curli-producing (YMel) and curli-deficient (YMel-1), were used.[14,15] Curli are surface organelles of *E. coli*, which are composed of thin fibers with a diameter of approximately 2 nm that mediate binding to adhesive proteins specific to fibronectin and laminin found in the eucaryotic extracellular matrix.[16] The significant role of curli in biofilm formation on a fibronectin-precoated substrate was clearly demonstrated.

MATERIALS AND METHODS

Bacterial strains and plasmid

The *E. coli* strains used in this study were the curli-producing strain YMel and the curli-deficient isogenic mutant strainYMel-1, both of which were transformed by electroporation with the *gfp*mut3* gene encoding plasmid DNA (pJBA27) and expressing a stable green fluorescent protein (Gfpmut3*) as previously reported.[17] *E. coli* from the frozen bacterial solution was cultured in 3 mL of modified Luria-Bertani medium containing 50 μg/mL ampicillin and 3 g/L NaCl at 37°C for 18 h under aerobic conditions, and then scaled up to a concentration of approximately 2×10^8 colony forming units per milliliter (CFU/mL), which was determined by the plate count method. Then they were diluted to a concentration of 2×10^5 CFU/mL, which was used as an initial concentration for experiments.

CLSM

The biofilms were examined by CLSM (Radiance 2000; BioRad, Hercules, CA). Square PU sheets (obtained from Olympus Optical Co., Ltd., Tokyo, Japan), which were cut to fit a six-well cell culture cluster, were sterilized using ethylene oxide, placed in a six-well cell culture cluster using sterilized forceps, and incubated with *E. coli* cell suspension (2×10^5 CFU/mL) under static condition. After 3-, 6-, 12-, and 24-h incubations, culture medium was removed and phosphate-buffered saline (PBS) was gently added to prevent drying of the biofilms. To visualize the EPS of the biofilms, rhodamine-labeled concanavalin A (5 μg/mL; Vector Laboratories, Burlingame, CA), which specifically binds to D-(+)-glucose and D-(+)-mannose groups on EPS, was used. One hundred microliters of this fluorescent solution was carefully applied on top of the biofilms grown on the PU sheet. After a 30-min incubation in the dark at room temperature, the excess staining solution was removed by four rinses with PBS. Images were recorded at an excitation wavelength of 488 nm and an emission wavelength of 515 ± 30 nm for GFP and at an excitation wavelength of 514 nm and an emission wavelength of 600 ± 50 nm for rhodamine-labeled concanavalin A.

Electron microscopy

For negative staining, *E. coli* cells, harvested from the biofilm formed on the PU sheet after a 24-h incubation, were mixed with distilled water, and the suspension was allowed to sediment for 2 min on a grid. After washing with distilled water, the specimen was negatively stained with 2% uranyl formiate and air dried before transmission electron microscopy (H-7000E; Hitachi, Tokyo, Japan).

For scanning electron microscopy (SEM), the biofilm grown on a glass slide (Matsunami Glass Industries Ltd., Osaka, Japan) after a 24-hr incubation was fixed in 2% glutaraldehyde (Electron Microscopy Sciences, Hatfield, PA) in 0.1*M* phosphate buffer for 1 h at room temperature. The fixed samples were dehydrated for 20 min at each step in an ascending acetone series, sputter-coated with platinum, and evaluated by SEM (JSM-840A; JEOL, Tokyo, Japan).

Bacterial adhesion study

The adhesion of bacteria was studied under static condition. Round PU sample sheets sterilized by ethylene oxide were placed in a 24-well cell culture cluster using sterilized forceps and incubated with *E. coli*. After 3-, 6-, 12-, and 24-h incubations, the round PU sheets were rinsed with PBS,

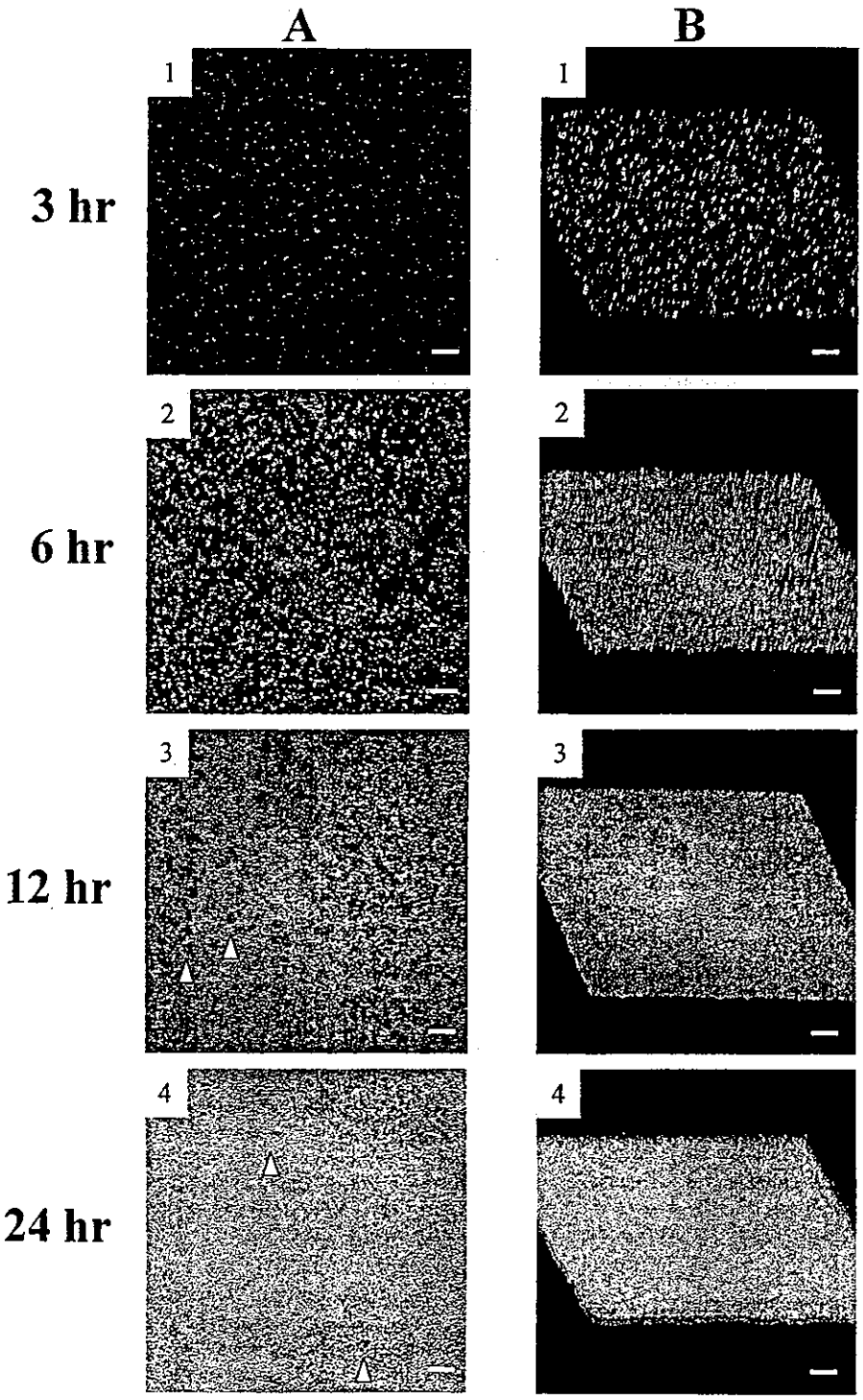

Figure 1. CLSM photographs of biofilms on PU at 3, 6, 12, and 24 h of incubations. (A) top view; (B) oblique view. Bar: 100 μm. Green and red areas indicate *E. coli* (expressing GFP) and EPS (stained with rhodamine-labeled concanavalin A), respectively. Irregular dark spots indicate water channels (white arrowheads).

placed in 15-mL Eppendorf tubes with 2 mL of PBS and sonicated for 60 s. Complete detachment of bacterial cells from the round sheets after 60-s sonication was confirmed by CLSM. Then, 100 μL of the solution containing detached bacterial cells was placed in a 96-well cell culture cluster and fluorescence intensity was measured with Molecular Imager FX (BioRad). Viable bacterial cells (CFU/cm^2) were also counted by the plate count method. Experiments were run with five samples, and the mean and standard deviation were recorded.

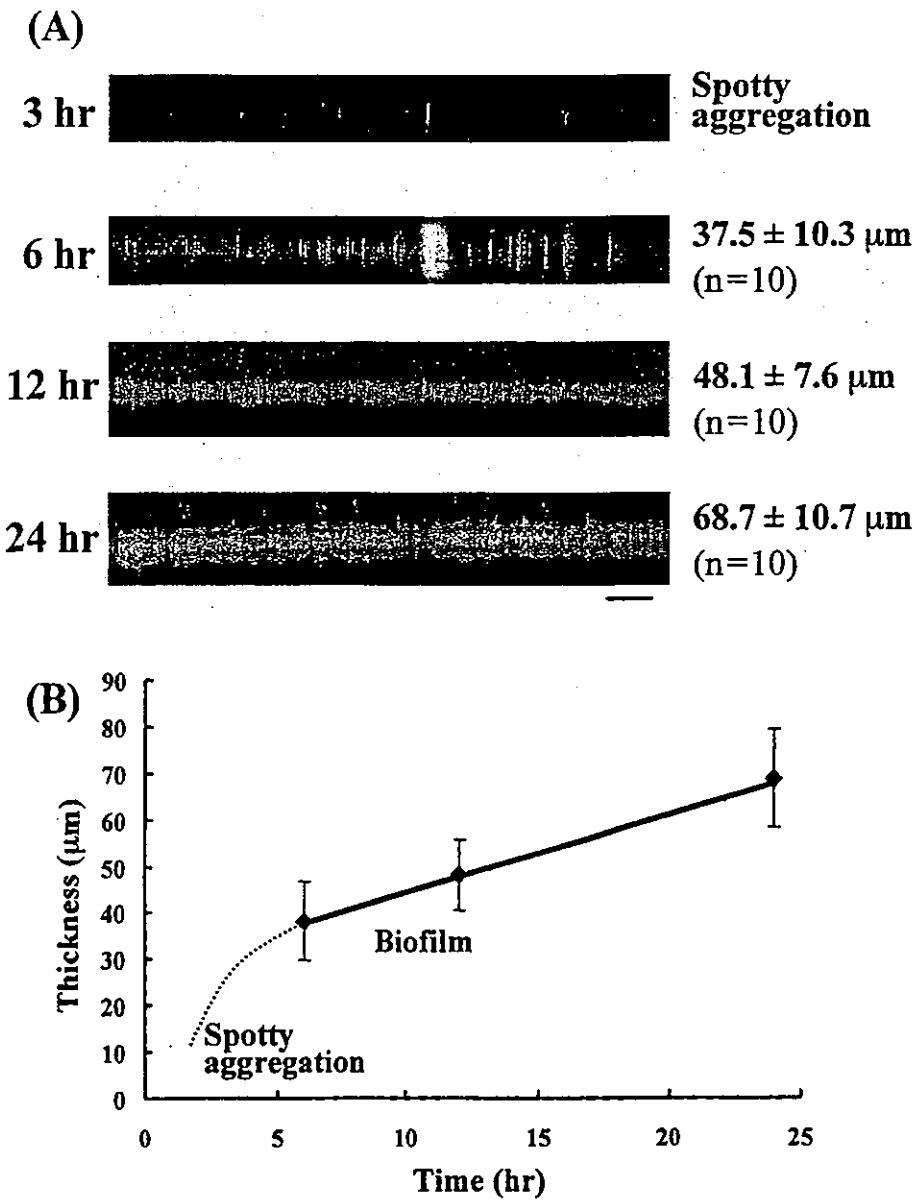

Figure 2. (A) CLSM photographs of vertical section of biofilms on PU at 3, 6, 12, and 24 h of incubations. Bar: 100 μm. (B) Biofilm thickness was determined by measuring the present images at 3, 6, 12, and 24 h of incubations. Ten vertical lines were randomly chosen for the analysis of each image. Values are expressed as means ± SD.

Protein coating of materials

Round PU sheets were incubated with bovine fibronectin (Itoham Foods Inc., Hyogo, Japan), bovine vitronectin (Yagai Co., Yamagata, Japan), and bovine serum albumin (Itoham Foods) at 1 mg/mL (0.1%) at 37°C for 24 h. Then, Luria-Bertani medium containing *E. coli* (2×10^5 CFU/mL) was poured over the protein-precoated round PU sheets and adherence was examined.

Statistical analysis

Statistical analysis was performed with the StatView 5.0 program (Abacus, Berkeley, CA). Data are shown as means ± SD. Statistical analysis was performed by analysis of variance. Differences at $p < 0.05$ were considered significant.

RESULTS

CLSM observation

To observe the 3D structure of the biofilm formed on the PU film, GFP-expressing YMel was cultured on the substrate under static condition for up to 24 h. After gentle washing with PBS, EPS generated during

biofilm formation was stained with rhodamine-labeled concanavalin A. The biofilm was observed using CLSM with time. Figure 1 shows (A) top-view and (B) oblique-view images of biofilms. At 3 h of incubation, adhered YMel cells (green color) randomly distributed without aggregate formation, and the EPS (red) formed regionally exhibited a thin cloudlike structure. At 6 h of incubation, the number of adhered YMel cells increased to form heterogeneous mosaic colonies composed of small aggregates that are scattered all over the substrate, and high-intensity red EPS regions tended to enlarge to cover the majority of the surface, thus initiating the formation of 3D structural constructs. The coexisting regions composed of green cells and red EPS were observed as a yellow region [Fig. 1(2B)]. At 12 h of incubation, the surface was completely covered with green (a major continuous matrix phase), yellow, and some spotty red regions (a dispersed domain). A small number of irregular dark spots were observed, which are supposed to be water channels, as described in the Discussion section. At 24 h of incubation, almost the entire surface area was yellowish-green, and the oblique-view CLSM image suggests that a thick biofilm was formed.

Figure 2(A) shows the time-lapse images of the vertical sections of biofilms. At the initial phase, spotty aggregates and single cells, which scattered horizontally but elongated vertically, were observed. At 6 h of incubation, the number of aggregates increased horizontally and formed a filmlike structure which enabled thickness measurement. At 12 h of incubation, the biofilm appeared more tightly packed. At 24 h of incubation, the vertical cross-sectional image revealed that EPS (yellow area) are predominantly located in the midlayer of the biofilm. To examine change in thickness with time, 10 vertical lines were randomly chosen for the measurement on each image for 6-, 12-, and 24-h incubations. Figure 2(B) shows that the average thickness of biofilms gradually increased with incubation time within the experimentally observed period.

Electron microscopic observation

The biofilm grown on glass for 24 h was observed using SEM. Figure 3 shows that *E. coli* and EPS, the matrix of the biofilm, formed a complex 3D structure. Irregularly shaped spaces resembling water channels were observed among dense structures. To confirm the expression of curli, which specifically bind to fibronectin and laminin, on the surface of *E. coli* YMel in the biofilm, negative staining was performed. Figure 4 shows a fine structure composed of thin fibers that suggest curli expression in YMel, but such a structure was not found in the curli-deficient mutant YMel-1.

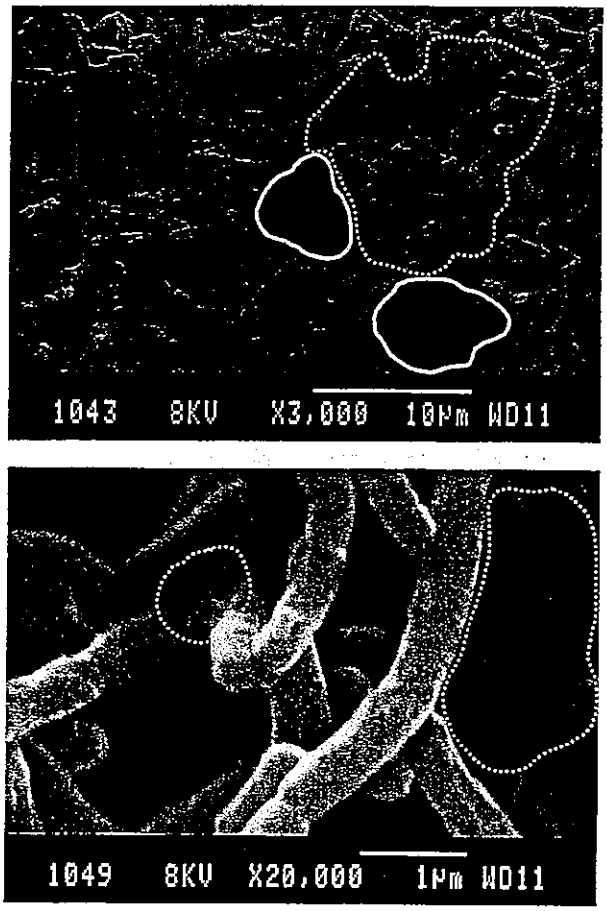

Figure 3. SEM photographs of biofilm on a glass slide at 24 h of incubation. Solid and broken lines indicate water channel regions and the dense parts of the biofilm, respectively.

Quantitative analysis

To quantify YMel cells that adhered to the PU film, round PU sheets that were incubated with YMel cells for up to 24 h postplating under static condition were subjected to gentle washing with PBS to remove nonadhering YMel cells, and then sonicated in PBS to detach all the adhered YMel cells. The fluorescence intensity of PBS containing detached YMel cells was measured with a fluorometer. In principle, the fluorescence intensity derived from GFP should correlate with the number of detached viable YMel cells by the plate count method. In fact, as shown in Figure 5, the fluorescence intensity highly correlated with the number of viable cells (correlation factor: 0.9997). The effect of the initial concentrations of YMel cells (2×10^3, 2×10^4, and 2×10^5 CFU/mL) on proliferation was studied (Fig. 6). The fluorescence intensity of PBS containing detached YMel cells increased as the initial cell concentration increased for up to 12 h of incubation. The higher the initial cell concentration, the higher the growth rate. However, after 12-h incubation, the flu-

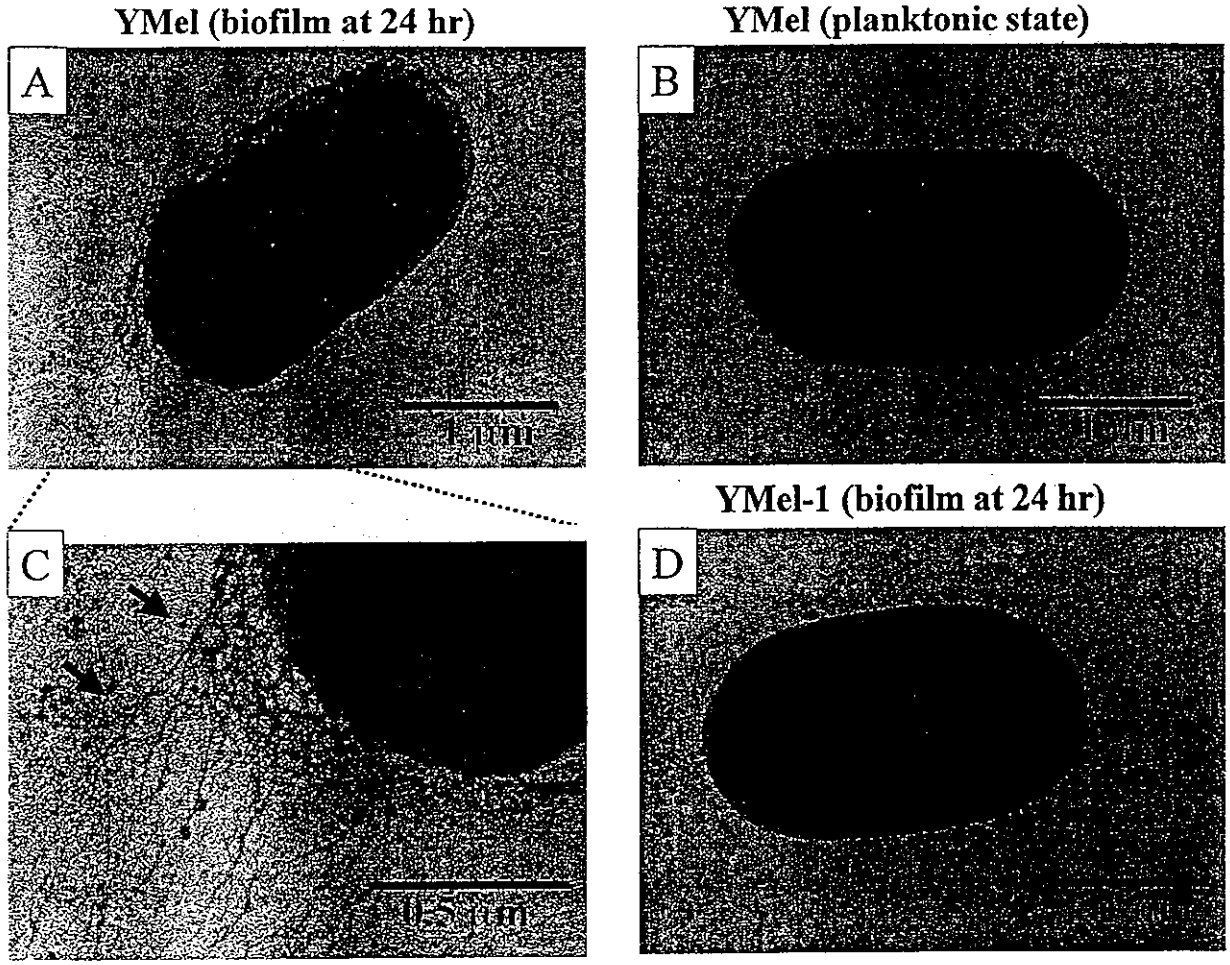

Figure 4. Transmission electron microscopic photographs by negative staining. (A) YMel in biofilm at 24 h; (B) YMel in planktonic state; (C) YMel in biofilm at 24 h with high magnification; and (D) YMel-1 in biofilm at 24 h. Arrows demonstrate curli.

orescence intensity remained almost constant, irrespective of the initial cell concentration.

Precoated-protein-dependent bacterial adhesion

To evaluate the effect of precoated proteins on bacterial adhesion, YMel was examined on round PU sheets precoated with the following proteins: fibronectin, vitronectin, and albumin (note that fibronectin and vitronectin are cell-adhesive, and albumin is non-cell-adhesive). As shown in Figure 7, for up to 12 h of incubation, there was a small significant difference in the number of adherent cells, irrespective of the type of precoated protein. However, at 24 h of incubation, the difference in the number of adherent cells was noted. The highest cell proliferation was observed on the fibronectin-coated surface, followed by the vitronectin-coated one, the proliferation potential of which was slightly higher than the noncoated surface; how-

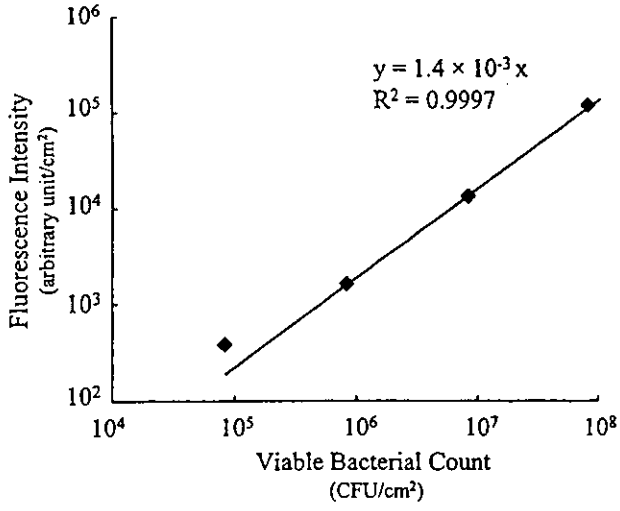

Figure 5. Correlation between fluorescence intensity and viable bacterial count in bacterial adhesion study at 24 h of incubation. The solution containing *E. coli* detached from PU sheets was diluted to different concentrations. Values are expressed as means ± SD.

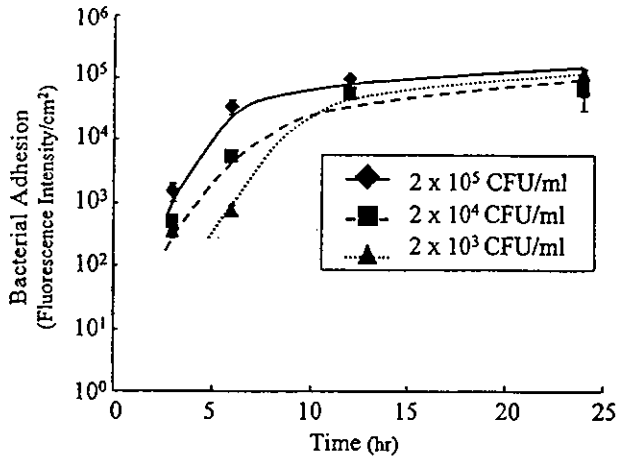

Figure 6. Time-dependent adhesion and proliferation of *E. coli* on PU. Initial concentration of bacterial cells: 2×10^3 (▲), 2×10^4 (■), 2×10^5, (◆) CFU/mL (n = 5). Values are expressed as means ± SD.

ever, there is only a small statistical difference between them. For the albumin-coated surface, although its initial adhesion potential is almost the same as that of the adhesive-protein-coated surfaces, minimal proliferation occured even with prolonged incubation time.

The curli-deficient mutant strain YMel-1 was used to determine the role of curli in bacterial adhesion. The curli-producing strain, YMel, and the curli-deficient isogenic mutant strain, YMel-1, were examined on PU surfaces with or without fibronectin coating. The number of adherent cells, measured by the plate count method, shows that the adhesion of YMel-1 was less than that of YMel to both fibronectin-coated and noncoated substrates. Precoating the PU sheets with fibronectin did not increase the adhesion of YMel-1 (Fig. 8), indicating that curli participate in fibronectin-mediated bacterial adhesion.

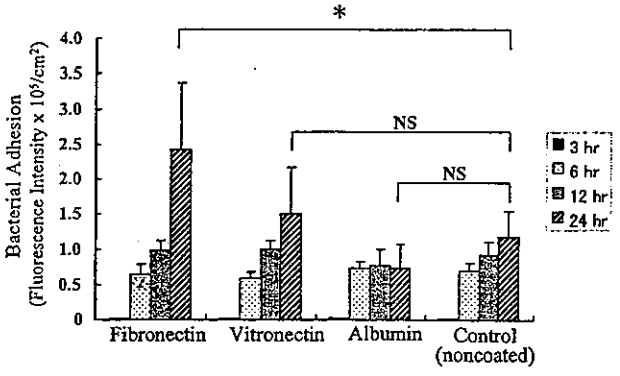

Figure 7. Bacterial adhesion to and proliferation on PU precoated with proteins at 3, 6, 12, and 24 h of incubations (n = 5). Control is noncoated PU. Values are expressed as means ± SD.

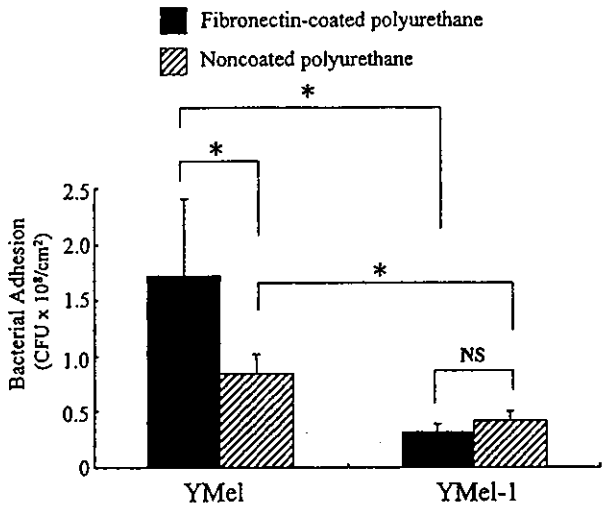

Figure 8. Bacterial adhesion and proliferation of curli-producing strain, YMel, and curli-deficient isogenic mutant strain, YMel-1 in fibronectin-coated PU and noncoated PU at 24 h of incubation (n = 5). Adhesion was determined by the plate count method. Values are expressed as means ± SD.

DISCUSSION

Bacterial adhesion is an important initial step in infection at the site of implanted biomaterials, which often causes life-threatening events in clinical situations.[1,2] Among bacteria capable of foreign-body-induced infection, *E. coli* is an important pathogen in the blockade of biliary stents or urinary catheters. The understanding of biofilm formation on synthetic biomaterials and the quantitative detection method for biofilm are key issues leading to the surface design of biomaterials with a high antibacterial adhesion potential. Electron microscopy has been used to examine biofilms on various materials.[9] However, sample preparation for electron microscopic observation requires sample dehydration, during which biofilms are often easily collapsed, structurally damaged, or destroyed. These dehydrated samples provide a deceivingly simplistic view of biofilms.[10]

To overcome this problem, we utilized fluorescent-compound-labeled *E. coli* strains that were transformed with a plasmid harboring the gene encoding GFP from jellyfish *Aequorea victoria* as an *in situ* cell marker. EPS are mainly responsible for the morphology and function of biofilms, and are considered to be key components that determine the physicochemical and biological properties of biofilms.[10,18] The co-use of GFP for bacteria and a fluorescent-compound-labeled marker specific to EPS in CLSM study provides new insights into the structure and nature of biofilm formation.

In our study, the imaging of 3D fine structures was acquired using fully hydrated samples for CLSM without any complex fixation such as the dehydration